A Chirp Spread Spectrum Modulation Scheme for Robust Power Line Communication

Stephen Robson, *Member, IEEE*, and Manu Haddad, *Member, IEEE*

***Abstract*—This paper proposes the use of a LoRa like chirp spread spectrum physical layer as the basis for a new Power Line Communication modulation scheme suited for low-bandwidth communication. It is shown that robust communication can be established even in channels exhibiting extreme multipath interference, impulsive noise and low SNR (−40 dB), with synchronisation requirements relaxed compared to conventional LoRa. ATP-EMTP simulations using frequency dependent line and transformer models, and simulations using artificial Rayleigh channels demonstrate the effectiveness of the new scheme in providing load data from LV feeders back to the MV primary substation. Our results demonstrate error-free communication at SNRs of −40 dB, and can be further improved by trading-off data rate. We further present experimental results based on a Field Programmable Gate Array hardware implementation which match the simulated performance.**

***Index Terms*—PLC, LoRa, LV monitoring.**

I. Introduction

DISTRIBUTION Network Operators (DNOs) already deploy a wide range of communication technologies to support the move towards smart grids. Advances in the standardisation of narrowband Power Line Communication (PLC) solutions such as Prime and G3-PLC, and growing options in long range wireless communication (i.e. LoRa) have only added to the options in the last decade. But there remains an unmet requirement for low-cost and robust communication of, for example, load data from secondary substations. The problem is amplified by the sheer number of required monitoring points (typically tens of thousands in a large regional distribution network) and the fact that secondary substations are often located in rural areas with limited access to conventional wired or wireless communication infrastructure.

Previous attempts at providing widescale communication across large distribution networks have tended to focus on the use of conventional wired media (i.e. ethernet), wireless solutions (LoRa, GSM) or PLC.

Narrowband PLC solutions such as Prime [1] and G3-PLC [2] are now firmly established on Low-Voltage (LV) networks, and are often deployed in automatic meter reading (AMR) applications and increasingly in support of other smart grid services. Over longer distances and across voltage levels, these technologies struggle to cope with the increased attenuation and extreme multipath conditions associated with transmission through transformers and Medium Voltage (MV) networks [3]. Some have proposed the use of spread spectrum techniques for use on the powerline channel due to its inherent resistance to multipath effects and low power [4][5], but a modulation scheme capable of traversing the LV-MV network reliably is needed. New technologies are required in this space.

This paper proposes a PLC modulation scheme based on the Chirp Spread Spectrum (CSS) scheme of the recently standardised LoRa physical layer [6]. The modification is designed to combat the two major problems of extreme multipath and low SNR. The former is resolved by subdividing the LoRa symbol into a reduced set, thereby containing the multipath energy into a single symbol. The latter is resolved through the use of statistical averaging of the modified signal over consecutive symbols. This trading off of data rate for performance makes possible a communication scheme in which many LV feeder monitoring devices can communicate back to a primary substation at timescales of several seconds or minutes.

II. Background

A. Requirements for Robust Communication on the LV-MV Channel

The communication channel linking the LV and MV parts of a distribution network is characterised by extreme multipath conditions (σ_{rms} = 10's to 100's of μs). The main contributing factor to this is not the attenuation of the power line itself, rather it is a result of delayed versions of the signal reaching the receiver from many different paths. On the MV network, the typical lengths of the line become much larger than the wavelength of the narrowband PLC signal, and lines are terminated by open circuits or transformers with large reflection coefficients. Therefore, much of the signal energy remains in the power line until it dissipates. Empirical measurements of the RMS delay spread on MV distribution networks is in the tens of μs [7]. In contrast, the RMS delay spread on LV networks is less than 10 μs [8]. Therefore, a robust communication scheme suited to this environment must accommodate extremely high RMS delay spreads, far beyond what is typical in LV and conventional wireless systems.

Manuscript received 3 September 2021; revised 21 February 2022; accepted 8 May 2022. Date of publication 27 May 2022; date of current version 28 November 2022. Paper no. TPWRD-01329-2021. *(Corresponding author: Stephen Robson.)*

The authors are with the Advanced High Voltage Engineering Research Centre (AHIVE), Cardiff University, CF24 3AA Cardiff CF24 3AA, U.K. (e-mail: robsons1@cardiff.ac.uk; haddad@cardiff.ac.uk).

Color versions of one or more figures in this article are available at https://doi.org/10.1109/TPWRD.2022.3175830.

Digital Object Identifier 10.1109/TPWRD.2022.3175830

When considering cross-network (LV-MV) transmission, for example in a system which relays load information from a secondary to a primary substation, a second major problem emerges. Though it has been demonstrated that PLC signals in the narrowband range (15-500 kHz) can indeed propagate through transformers, the attenuation is large. Empirical measurements show an average 35 dB attenuation with a high degree of frequency selectivity [9]. The SNR penalty imposed by this scale of attenuation renders existing narrowband PLC technologies unusable. The situation is further exacerbated by regulatory limits on transmit power on power lines. Therefore, reliable inter-transformer communication is only possible with communication schemes that can work at low SNRs.

The low SNR regime is usually defined with reference to Additive White Gaussian Noise (AWGN). However, the power line channel has also been shown to be associated with impulsive noise [10]. Mitigation techniques exist for OFDM-based PLC techniques, including clipping [11], [12] and iterative techniques [13].

The dual problem of extreme multipath and high attenuation, exacerbated by both AWGN and impulsive noise, makes the design of a communication system for this channel extremely challenging. Recently, the emerging LoRa standard was proposed for PLC communication [14], and then for time disemmination [15][16]. LoRa has several favourable properties, including excellent receiver sensitivity and low power. However, in its raw form, it performs poorly in severe multipath. Here, we exploit the unique properties of LoRa, with a few key modifications, for robust performance in the low SNR and high multipath regime.

B. The LoRa Physical Layer

The mathematical basis underpinning the LoRa physical layer has been studied extensively in several recent works [17][18] [19]. LoRa transmits symbols as frequency shifted chirps. With a bandwidth of $B = \frac{1}{T}$, the transmitted symbol, w_k is defined as:

$$w_k(nT) = \sqrt{\frac{E_s}{2^{SF}}} e^{j2\pi\cdot(k+n) \mod 2^{SF}\cdot\frac{n}{2^{SF}}} \tag{1}$$

The above equation describes a series of $n = 0, 1, 2 \ldots 2^{SF-1}$ consecutive samples forming a LoRa symbol. $SF \in \{7, 8 \ldots, 12\}$ is the so called Spreading Factor, which determines the number of transmitted samples per LoRa symbol. $k \in 0, 1, 2 \ldots 2^{SF-1}$ is the transmitted symbol and E_s is the symbol energy. It has been shown in [17] that the 2^{SF} basis functions are orthogonal allowing a sufficiently synchronised receiver to demodulate using correlation. If r_k is the received symbol corrupted by Additive White Gaussian Noise (AWGN), ϕ_i, and w_i^* is the complex conjugate of symbol k (i.e. that corresponding to the transmitted symbol), the correlator output y will exhibit a peak at index k.

$$\sum_{n=0}^{2^{SF-1}} r_k(nT)\cdot w_i^*(nT) = \begin{cases} \sqrt{E_s} + \phi_i & i = k \\ \phi_i & i \neq k \end{cases} \tag{2}$$

$$y_k = \arg\max\left(\left|\delta_{k,i}\sqrt{E_s} + \phi_i\right|\right) \tag{3}$$

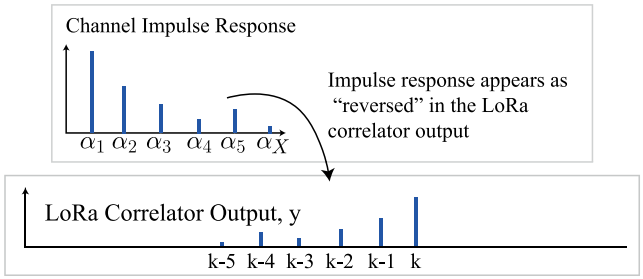

Fig. 1. The correlator output resulting from transmission in a multipath channel.

It is demonstrated in [17] how the more computationally efficient method removes the need to perform the full correlation over all 2^{SF} basis functions. Indeed, the method used by LoRa requires only the multiplication of r_k with the complex conjugate of the base down chirp (a process known as dechirping). The dechirped signal comprises a pure frequency tone which is proportionate to k, so an FFT and find max routine completes the demodulation process.

Equation (2) shows that correct demodulation will take place when $\sqrt{E_s} + \phi_k$ exceeds the maximum value of ϕ across all correlations. Although there may be significant distance between the PDFs of ϕ and $\sqrt{E_s} + \phi_k$, it is actually the PDF of the maximum of ϕ per symbol that is of interest in Symbol Error Rate (SER) calculations.

C. Performance of LoRa in Multipath Channels

In most conventional LoRa applications, the RMS delay spread is in the ns or low μs range. This contains the majority of the multipath energy within a single sample and can be considered as frequency flat fading. However, in PLC applications, delay spreads of several tens of μs have been recorded. In this case, the multipath energy will smear across samples and will be more appropriately modelled as frequency selecting fading. A basic model of the situation can be constructed in which delayed versions of the transmitted symbol arrive at the receiver. Due to the unique way LoRa is modulated - effectively as time-shifted versions of a base chirp - a delayed version of a transmitted symbol will be demodulated as if it belonged to an adjacent symbol, as shown in (4), where index $i = k - 1 \ldots k - x$ are proportionate to $\alpha_2 \ldots \alpha_x$, where α is the impulse response of the channel. This is shown graphically in Fig. 1.

$$\sum_{n=0}^{2^{SF-1}} r_k(nT)\cdot w_i^*(nT) = \begin{cases} \sqrt{\alpha_1 E_s} + \phi_i & i = k \\ \sqrt{\alpha_2 E_s} + \phi_i & i = k-1 \\ \vdots & \vdots \\ \sqrt{\alpha_x E_s} + \phi_i & i = k-x \\ \phi_i & \text{elsewhere} \end{cases} \tag{4}$$

Therefore, the channel impulse response can be mapped out from the correlator output. In standard LoRa modulation, the presence of strong multipath interference in which the signal arrives by one or more indirect paths presents a problem for the LoRa demodulator because strong correlation peaks caused by

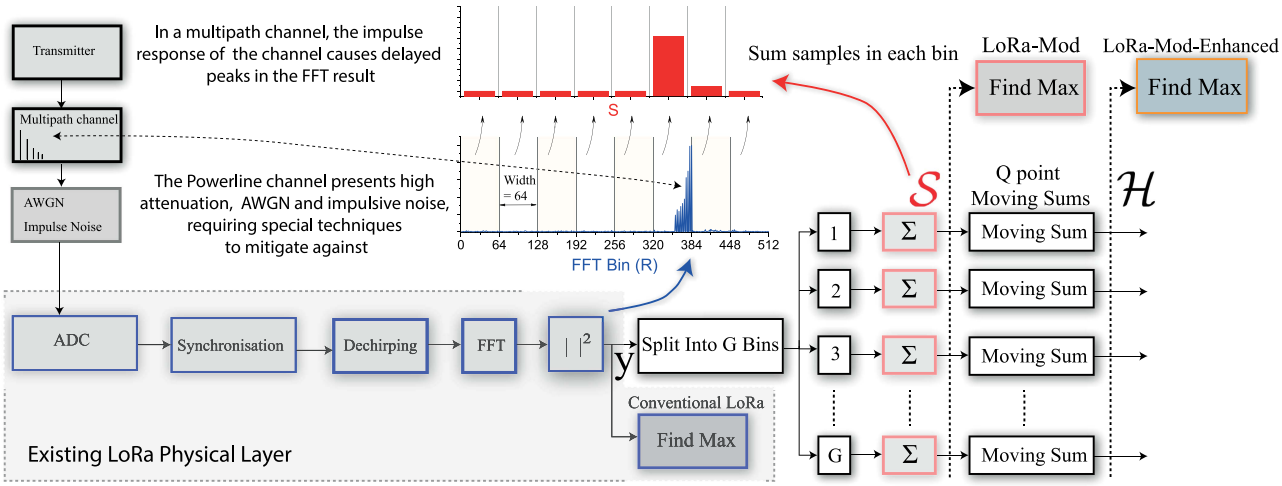

Fig. 2. Schematic diagram showing the proposed receiver architecture. The deviation from conventional LoRa starts at the "Split into G Bins" block. This subdivides the 2^{SF} bins into a reduced set of $G = \frac{M}{P}$ bins.

these paths will compete against the true transmitted symbol, raising the SER.

III. Description of the Proposed Method

A. Enhancement for Robustness in Extreme Multipath

1) description of Lora-Mod: It is interesting to note that the correlator output of the LoRa demodulator mimics the channel impulse response. This was noted in [20], which exploits the regularity of the channel impulse response across subsequent LoRa symbols through the use of cross-correlation. This method would be particularly interesting in PLC applications because the channel is fixed. However, the performance is similar to that of conventional LoRa systems in the AWGN channel, which is still not good enough to perform reliably on the particularly hostile LV-MV channel. We also remark that the synchronisation requirements match that of conventional LoRa, which is difficult to achieve on the power line channel.

In the proposed method, which is shown graphically in Fig. 2, the convenient grouping of multipath energy into a predictable place in the correlator output is exploited in a different way. If the correlator output is termed $y(k)$, where each term in y represents the absolute value of one of 2^{SF} output bins of the FFT operation, we can group the bins into a reduced set of g 'superbins'.

Assuming that the length of the channel impulse response is significantly smaller than the symbol time, T_s, the set of M possible symbols can be reduced to a smaller set of $G = \frac{M}{P}$ possible symbols, each encoding $SF - \log_2 P$ bits, where $P \in 2^{\mathbb{Z}}$ is the number of samples in each superbin. The modulator now encodes into a reduced set of $g \in 0 \ldots G-1$ possible positions. If PT_e is longer than the channel impulse response, the spread of energy resulting from multipath interference will be contained to a single superbin. To implement this scheme at the transmitter, data should be encoded into one of a set of possible symbols described by $m^g \in P, 2P, \ldots GP$. The restricted set of symbols are separated by P samples, which, if longer than the manifestation of the channel impulse response within R_m, will contain the multipath energy to within the symbol being transmitted.

At the receiver, the process is identical to standard LoRa demodulation except that a reduced set of G symbols are derived from the sum of the previous P bins:

$$S(g) = \sum_{n=(g-1)P}^{gP} |y(n)|^2 \tag{5}$$

Equation 5 shows a set of S output terms, with each term representing the sum of P correlator output terms from the FFT output, y. The summation combines the multipath energy within the symbol into a single number. The receiver can commence to finding the maximum index within S in the same way as the conventional LoRa demodulation process finds the maximum y. Equation 4 shows that y is made up of the square root of the symbol energy ($\sqrt{E_s}$) when $i = k$ (in the case of LoRa transmission in the AWGN channel) and a dispersed share of the symbol energy when $k - x \geq i \leq k$ in the case of transmission on the multipath channel with a delay spread of x samples. Every term in y is also made up of a complex zero-mean Gaussian noise process, ϕ.

The find max routine must now choose from a reduced set of terms. The energy in each term is now made up of the sum of P noise terms and, in the case of the correct symbol, the dispersed symbol energy. If the condition that $P \cdot T_e > \sigma_{rms}$, the majority of the symbol energy will fall within a single term. Therefore, the find max routine can still demodulate the symbol even in multipath channels, albeit at the expense of a reduced data rate.

Each superbin comprises the sum of P squared noise term samples, $|\phi|^2$, from the correlator output of Eqn. 4. Since $|\phi|$ is a Rayleigh distributed random variable, its square is distributed exponentially, and the sum of P of these samples follows a Gamma distribution. We have approximated this as a Gaussian distribution with μ equal to the expected value of the sum of

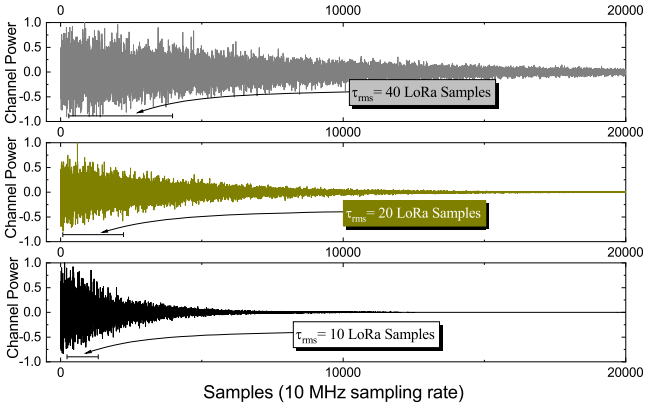

Fig. 3. Representation of the Rayleigh Fading Channels, shown here normalised to the maximum path. The RMS delay spread is defined in terms of LoRa samples to simplify the comparison with bin size.

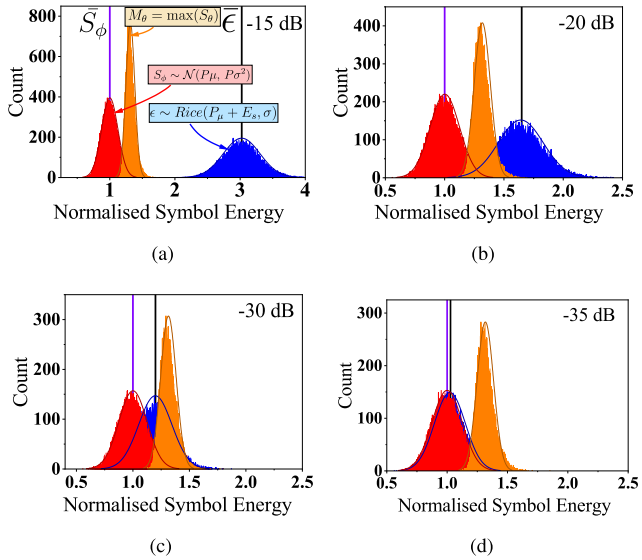

Fig. 4. Histograms: bin size = 64, 10 sample channel. (a) SNR = −15 dB (b) SNR = −20 dB (c) SNR = −30 dB (d) SNR = −35 dB.

the noise terms and σ equal to the sum of the noise variance, $S_\phi \sim \mathcal{N}(P\mu,\, P\sigma^2)$.

The superbin which corresponds to the correct symbol, $\mathcal{E}$, follows a Rician distribution with shape parameter $k_\beta = E_s/2\sigma^2 = E_s/N_0$, where N_0 is the single-sided noise power spectral density.

The demodulation process performs a find max routine which can be simplified as the comparison between $\mathcal{E}$ and the maximum of all other $g-1$ symbols. The distribution describing the maximum of $g-1$ normally distributed random variables is denoted M_ϕ. The expected value of M_ϕ can be approximated as $\sqrt{2\log(g-1)}$ standard deviations greater than the expected value of S_ϕ. A correct demodulation is achieved if $\mathcal{E} > M_\phi$.

2) channel Modelling: In a later section, a detailed ATP-EMTP model with frequency dependent line and transformer models will be used to simulate the proposed method in a realistic LV-MV scale case study. In this section, we begin by testing Lora-Mod in a 26,000-tap Rayleigh fading model. The motivations for using a Rayleigh fading channel are twofold. First, it is a channel model that is widely used in PLC modelling [21], [22]. Second, It is easy to replicate and control the duration of the RMS delay spread (τ_{rms}). In our simulations, the convolution between the transmitted signal and the Rayleigh channel is performed at 10 MHz then downsampled at the receiver to 100 kHz (the LoRa baseband). Therefore, the 26,000-tap Rayleigh channel is equivalent to 260 LoRa samples, though the RMS delay spread has been set to 10, 20 and 40 LoRa samples in the three scenarios. The three channels are shown in Fig. 3.

3) simulation Results for LoRa-Mod: Fig. 4 shows S_ϕ, M_ϕ and $\mathcal{E}$ resulting from 30,000 Monte Carlo simulations for a spreading factor of 12 and a bin size of 64. The 10 sample Rayleigh channel is used. Setting the bin size (64) greater than the RMS delay spread (10) guarantees that the majority of the symbol energy will fall within a single bin. The vertical reference lines labelled $\bar{S}_\phi$ and $\bar{\mathcal{E}}$ represent the means of the noise and transmitted symbol, respectively. The X scale is normalised to $\bar{S}_\phi$, and we retain this convention throughout the rest of the paper.

In Fig 4(a) (SNR = −15 dB), there is a clear separation between S_ϕ and $\mathcal{E}$. LoRa-Mod, which relies on a comparison between $\mathcal{E}$ and M_ϕ, can operate successfully at this SNR. Fig 4(b) (SNR = −20 dB) shows a more pronounced overlap between $\mathcal{E}$ and M_ϕ, which leads to an increasing symbol error rate for LoRa-Mod. Beyond this point, LoRa-Mod cannot be used. However, it is noted that the mean of $\mathcal{E}$ is still larger than the mean of S_ϕ, even at extremely low SNRs (e.g. in the case of −35 dB in Fig. 4(d)).

Fig. 5 shows the performance of LoRa-Mod in the three Rayleigh channels (τ_{rms} = 10, 20 and 40 LoRa samples) and for two different spreading factors (SF = 12, 14). Firstly, the general level of performance improves with increasing spreading factor. Secondly, the results confirm the requirement for the bin size to be at least as large as τ_{rms}. For example, in Fig. 5(a) and (b), which is the 10 sample channel, all superbin sizes perform relatively well. In the 20 sample channel (Fig. 5(b) and (d)), the 4, 8 and 16 sample bin size schemes exhibit a drop in performance. In the 40 sample channel, the trend continues.

B. Enhancement for Robustness in Extremely Low SNRs

1) description of LoRa-Mod-Enhanced: Lora-Mod has the flexibility to perform well in channels with arbitrarily long RMS delay spreads and poor SNRs, but a further trade-off of data rate can improve the performance to even lower SNR regimes. This scheme, termed Lora-Mod-Enhanced henceforth, uses the principle of statistical averaging to estimate the means of $\mathcal{E}$ and the noise symbol S_ϕ distributions. As shown in Fig. 2, this comes at the cost in hardware of a recursive running sum or running mean for each bin. Depending on the length of the moving average, the enhanced scheme also comes at the cost of an increased time-on-air.

In extremely low SNRs, the difference between the means of $\mathcal{E}$ and S_ϕ is small but non-zero. Should the same transmitted

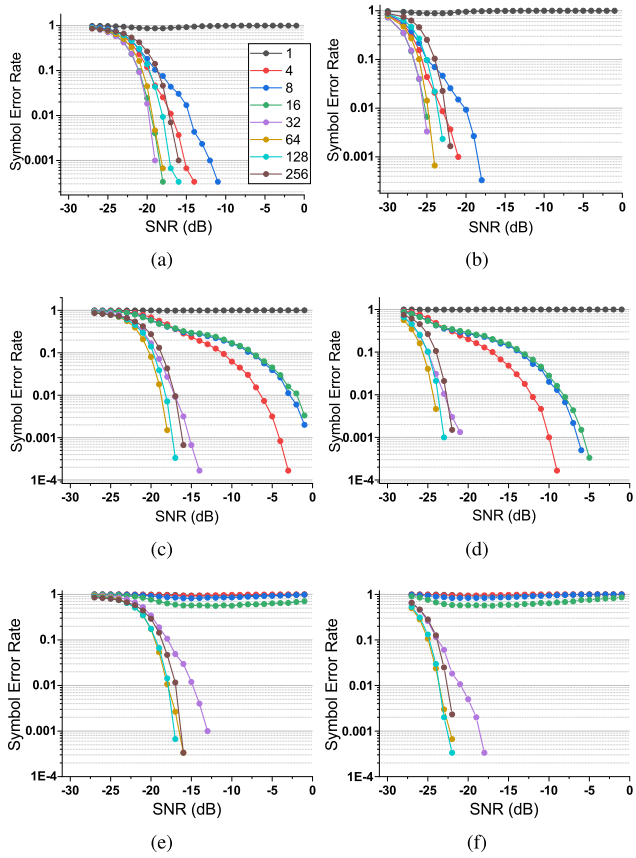

Fig. 5. Performance of LoRa-Mod: SNR Versus Symbol Error Rate as a function of superbin size, SF = 12, 14, and various length Rayleigh channels. (a) 10 sample channel SF = 12 (b) 10 sample channel SF = 14 (c)20 sample channel SF = 12 (d) 20 sample channel SF = 14 (e) 40 sample channel SF = 12 (f) 40 sample channel SF = 14.

symbol be repeatedly sent, the receiver can estimate the mean of the previous Q symbols of $\mathcal{E}$ (the transmitted symbol) and S_ϕ (all noise symbols). Unlike LoRa-Mod, which is a comparison between the maximum noise symbol (M_ϕ, shown in orange in Fig. 4), and $\mathcal{E}$, LoRa-Mod-Enhanced is a comparison between the mean of the previous Q $\mathcal{E}$ symbols with the maximum of the means of the previous Q S_ϕ symbols.

$$\mathcal{H}(g) = \frac{1}{Q}\sum_{n=0}^{Q} S(g-n) \tag{6}$$

The variance of $\mathcal{H}$ is narrowed compared to S_ϕ:

$$\bar{S_\phi} = H_\phi \sim \mathcal{N}\left(P\mu, \frac{P\sigma^2}{Q}\right) \tag{7}$$

Although the symbol error rate is still dependent on the comparison between the transmitted symbol and the maximum of the noise symbols, both terms have distributions which are significantly narrowed by the averaging. Since it can be guaranteed that most of the transmitted symbol energy will fall within $\mathcal{E}$, a high enough Q is able to detect the statistical difference between the two means, even at extremely low SNRs.

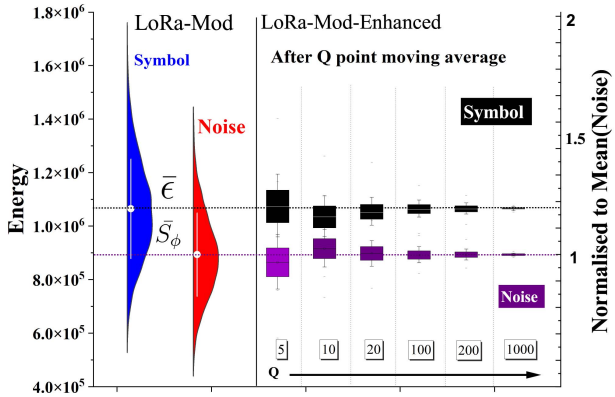

Fig. 6. Graphical demonstration of the working principle of Lora-Mod-Enhanced. In Lora-Mod, the Symbol energy is compared to the maximum energy of the remaining noise symbols. However, LoRa-Mod-Enhanced uses a Q-point moving average. The comparison is now between two distributions which are significantly narrowed, making error free communication in channels with extremely low SNRs (and significant multipath interference) possible.

This approach requires a compromise in terms of the maximum achievable datarate since, in effect, any gains made in robustness due to an increase in Q are matched by a proportionate reduction in datarate. However, in grid applications where load data is only required on the timescale of minutes, this compromise might be acceptable.

2) performance of LoRa-Mod-Enhanced With AWGN: Fig. 6 shows the narrowing of the symbol and noise distributions resulting from Q-point moving sums. In this case, Lora-Mod will not work because there is too much overlap between $\mathcal{E}$ and S_ϕ. However, in Lora-Mod-Enhanced, the difference between the symbol and the noise is more distinct and error-free communication is possible.

Fig. 7 shows the distributions (represented as horizontal lines) of normalised symbol energy for a spreading factor of 12 and for various bin sizes. It also shows the effect of varying the running mean length, Q. The same LoRa parameters deployed in Fig. 4 are used, meaning the majority of the multipath energy falls within the transmitted symbol superbin, $\mathcal{E}$. It is interesting to note that increasing the bin size beyond that which is necessary to contain the multipath energy actually deteriorates performance of LoRa-mod-enhanced, as indicated by the narrowing of the gap between the purple lines ($\bar{S_\phi}$ and the $\bar{\mathcal{E}}$).

The performance of LoRa-Mod-Enhanced (under the presence of AWGN and the 20 sample Rayleigh channel, SF = 14) is shown in Fig. 8. It is clear that the LoRa-Mod-Enhanced significantly outperforms Lora-Mod, and increasing the value of Q improves performance. It is also noted that the Bin=16 channel has lower performance than the Bin = 32, 64, 128 channels because the condition of Bin size $> \tau_{rms}$ is not met.

C. Performance of Lora-Mod-Enhanced in Channels With Impulsive Noise

1) development of an Impulsive Noise Model: It has been demonstrated through empirical measurements that the statistical properties of impulsive noise on the power line channel

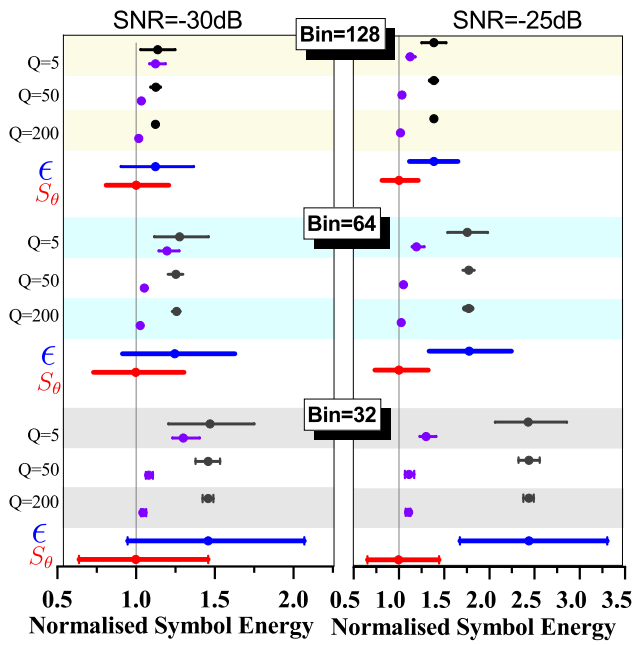

Fig. 7. Boxplots summarising the distributions of S_ϕ, $\mathcal{E}$ and $\mathcal{H}$ (LoRa-Mod-Enhanced) for Q = 5, 50 and 500 symbols. Increasing Q narrows the distribution of $\mathcal{H}$ and creates a wider normalised separation, making error free communication possible.

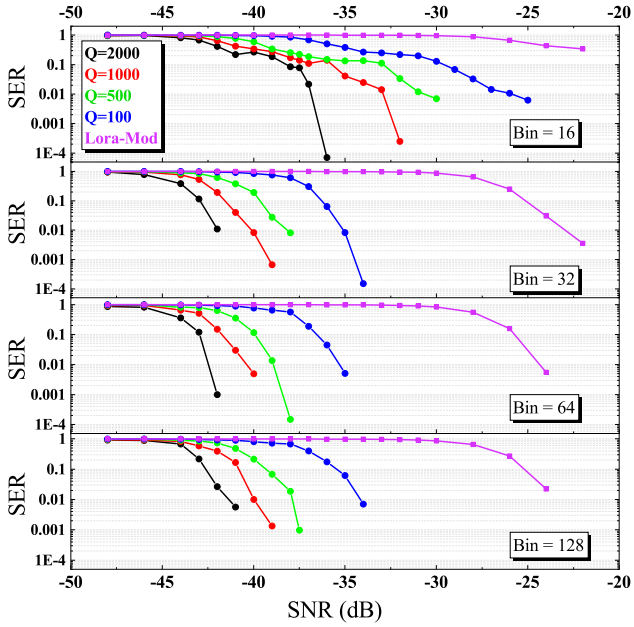

Fig. 8. Graph to show the improvement in performance with increasing Q at an SF = 14. The channel used here is the 20 sample Rayleigh channel.

are characterised to a good approximation by the α-stable distribution, S$(\alpha, \beta, \gamma, \delta)$ [23]. The 4 parameters of the α-stable distribution are described in Table I. It important to note that the Gaussian distribution is a special case of the α-stable distribution for $\alpha = 2$:

TABLE I
PARAMETERS OF THE α-STABLE DISTRIBUTION

Parameter	Description	Range
α	First shape parameter	$0 < \alpha \leq 2$
β	Second shape parameter	$-1 \leq \beta \leq 1$
γ	Scale parameter	$0 < \gamma < \infty$
δ	Location parameter	$0 -\infty \delta < \infty$

$$\mathcal{N}\left(\mu, \sigma^2\right) = S\left(2, 0, \frac{\sigma}{\sqrt{2}}, \mu\right) \tag{8}$$

Decreasing α below 2 leads to a distribution with heavier tails which increases the possibility of extreme values. In [24], indoor power line noise between 30 kHz and 500 kHz was measured in both China and Italy. The power line noise approximated well to an α stable distribution with α varying between 1.75 and 1.85 in Italy, and a more impulsive 1.22 to 1.63 in China. In [25], noise measurements at an industrial zone yielded an α of around 1.8. As noted in [24], the variance of the α-stable distribution for $0 < \alpha < 2$ is infinite, leading to the occassional (bot undesirable) sample from the very far ends of the tails far exceeding the maximum of the real impulsive noise. For this reason, [24] propose a thresholding method for removing extreme outliers, preserving a truncated portion of the α-stable distribution as a more accurate model of the noise:

$$N_{th} = \begin{cases} N_\alpha(n), & \text{if } |N_\alpha(n)| < T \\ T \cdot sgn(N_\alpha(n)), & \text{otherwise} \end{cases} \tag{9}$$

Where N_{th} is the noise sample after thresholding, N_α is the raw noise sample from the α stable distribution and T is the threshold.

2) application of Thresholding At the receiver: It is also noted that thresholding is a well-known technique in existing PLC systems as a mitigation against impulsive noise [10]. Unlike conventional PLC modulation schemes, the proposed method operates in the negative SNR regime. This means the signal is not distinguishable from the noise, so conventional threshold detection methods (e.g. those described in [11][12]) are not applicable. Therefore, we propose setting the threshold, T, to a multiple of the measured value of the noise. The larger this multiple, the higher the clipping threshold will be. We have arbitrarily chosen the 90^{th} percentile of the absolute value of the measured noise samples, N_{90}, to be be this measure. Therefore, T will be set to $N_{90} \cdot M$, where M is the multiple. Fig. 9 shows a sample of noise from the α stable distribution ($\alpha = 1.8$) and the effect of thresholding the noise to M times N_{90}, where in this case, M = 5.

3) definition of SNR: The variance of an α-stable distribution is infinite for $\alpha < 2$, meaning the normal definition of SNR is invalid. In this work, we have found the signal-to-dispersion ratio to be appropriate [26]:

$$SNR_D = 10 \log_{10} \frac{P}{2\gamma^2} \tag{10}$$

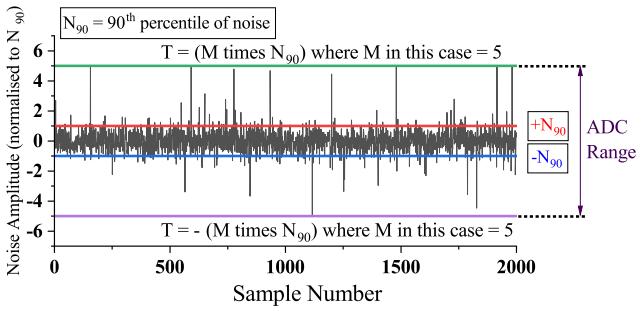

Fig. 9. Demonstration of the clipping tehchnique. Shown here is a noise signal sampled from α=1.8 distribution. In this case, M is chosen as 5, with sets a threshold of $\mathrm{M} \cdot \mathrm{N}_{90} = 5$. The signal is normalised to the 90^{th} percentile of the absolute value of the measured noise signal, N_{90}.

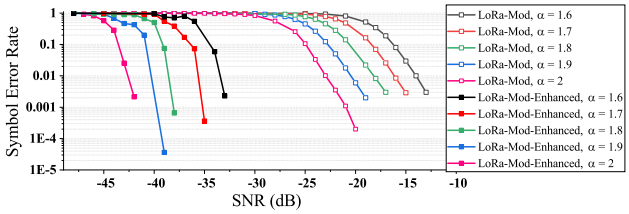

Fig. 10. Effect of Impulsive noise without clipping, Q = 2000, SF = 14, Bin = 64, 20-sample Rayleigh channel.

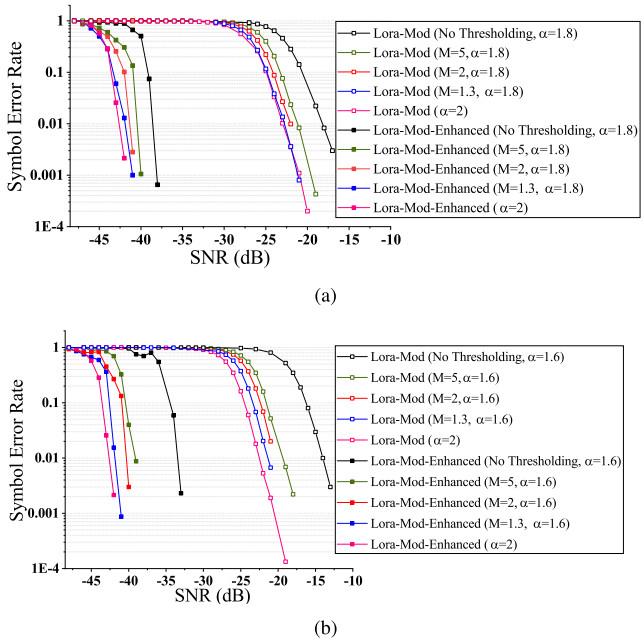

Fig. 11. Performance of Lora-Mod and Lora-Mod-Enhanced with clipping at M = 5,M = 2, M = 1.3 (Q = 2000, SF = 14, Bin = 64, 20-sample Rayleigh channel). The performance at $\alpha = 2$, and without thresholding, is also shown here as reference. It is observed that more aggressive thresholding exhibits better performance. (a) $\alpha = 1.8$ (b) $\alpha = 1.6$.

Where P is the signal power.

4) simulation Results Under Impulsive Noise: Fig. 10 shows the performance of Lora-Mod and Lora-Mod-Enhanced in the presence of Impulsive noise ($\alpha = 1.6$ and 1.8 are shown). Here, no clipping is used. It is observed that the performance drop is proportionate to the severity of the impulsive noise. Fig. 11 shows the performance of Lora-Mod and Lora-Mod-Enhanced in impulsive channels with various degrees of clipping (M = 5, 2, 1.3). The performance for no thresholding and a purely gaussian noise ($\alpha = 2$) are also shown for reference. It is observed that more aggressive thresholding is associated with better performance. At M = 1.3 (the most aggressive thresholding), the performance is similar to that of a purely gaussian channel. Therefore, we see no substantial deterioration in performance due to impulsive noise if an appropriate clipping routine is deployed.

D. Synchronisation

The synchronisation requirements are drastically relaxed in comparison to conventional LoRa because it does not matter if energy smears across LoRa bins (the energy will remain inside the superbin). This opens up the possibility of using zero-crossing detectors to estimate the start point of each symbol, reducing the complexity of both transmitter and receiver and removing the requirement for a preamble.

IV. Case Study

A. Development of a Test Network

The test network, as shown in Fig. 12, has 5 LV feeders and a radial MV network. The LV feeders use underground cable models (three-phase in an enclosed pipe) and the HV network comprises an overhead line based on an 11 kV wood pole model. All models use the frequency dependent JMarti model generated by the Lines and Cables Constants (LCC) routine of the EMTP. The MV/LV transformers are modelled with the high frequency Catallioti model [27] and each LV line is terminated on the load side by a three-phase 10 Ω resistance.

B. Simulation Methodology

Two LoRa-Mod-Enhanced devices are placed within each of the 5 feeders (labelled A-E in Fig. 12). A single receiver is placed near the primary substation (labelled 'O'). The modulation code, which is executed in Matlab, automatically writes each sample to a text file. This text file is read by a 'foreign model,' which is a custom piece of code executed natively within the EMTP, and provides the source signal for a TACS source. The process can be repeated for any number of TACS sources within the simulation, providing scope for a full system-wide simulation incorporating several transmitters. This methodology also resolves the challenge of writing many millions of samples into EMTP, and allows the communication signal to be read at the same ΔT as the simulation (1E-7). On completion, the EMTP simulation results are converted to a. MAT file using the PL42MAT routine and processed by the demodulation code within Matlab.

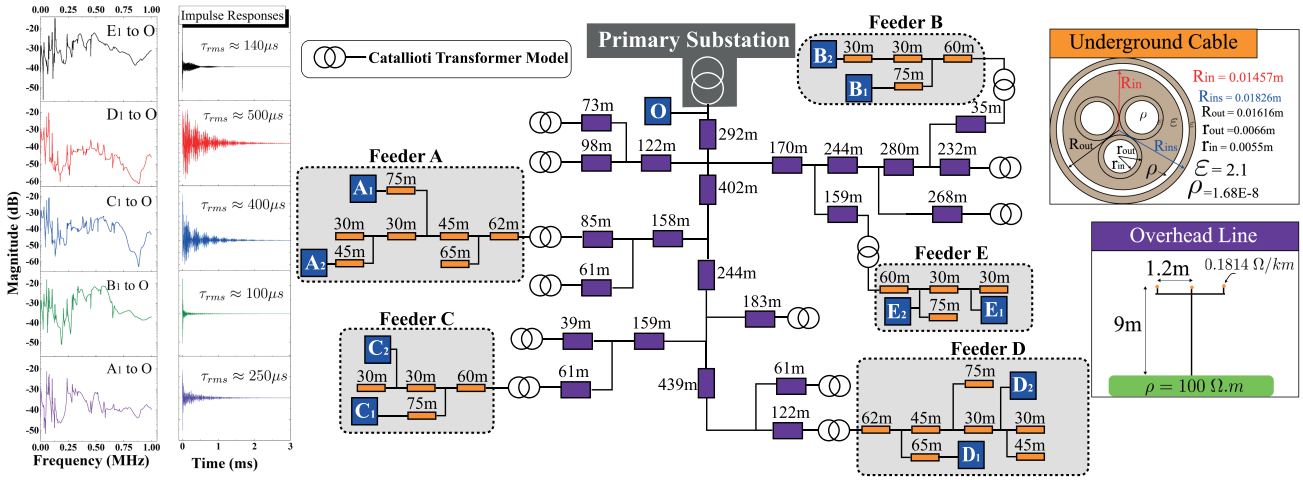

Fig. 12. ATP-EMTP Test Network comprising 5 LV feeders and a radial MV network.

TABLE II
SIMULATION PARAMETERS

Tx	SF	Time on Air (s) Q=1	Q=10	Q=100	f_c	BW
A_1	13	0.33	3.3	33	50 kHz	25 kHz
A_2	13	0.33	3.3	33	80 kHz	25 kHz
B_1	13	0.33	3.3	33	110 kHz	25 kHz
B_2	13	0.33	3.3	33	140 kHz	25 kHz
C_1	13	0.33	3.3	33	170 kHz	25 kHz
C_2	13	0.33	3.3	33	210 kHz	25 kHz
D_1	13	0.33	3.3	33	240 kHz	25 kHz
D_2	13	0.33	3.3	33	270 kHz	25 kHz
E_1	13	0.33	3.3	33	300 kHz	25 kHz
E_2	13	0.33	3.3	33	330 kHz	25 kHz

Fig. 12 also shows the magnitude and impulse responses between a selection of 5 transmitters and the observation point ('O'). The shape of these responses is representative of the MV power line channel, which is characterised by extreme multipath and regions of high attenuation. The RMS delay spread is observed to vary between 100 μs and 500 μs. In the context of a network-wide implementation of the proposed scheme, the magnitude responses show the importance of bandwidth selection. For example, fluctuations of just a few kHz exhibit differences of tens of dBs. Based on the criteria that the bin size should exceed the RMS delay spread of the channel, the bin size has been selected to be 64 (1.3 ms). This comfortably exceeds the maximum RMS delay spreads shown in Fig. 12. To model impulsive noise, an α stable distribution with $\alpha = 1.7$ is used, alongside a clipping threshold of M = 1.3.

C. Simulation Results

Fig. 13 shows the symbol error rate as a function of SNR for transmitters A1 to E1. At the chosen spreading factor (SF = 13) and the parameters shown in Table II, the results show that LoRa-Mod breaks down at an SNR of around −20 dB. However, LoRa-Mod-Enhanced continues to perform well up to −25 dB (Q = 10), −35 dB (Q = 100) and −39 dB (Q = 500). The results are similar across all transmitter points (E2 is not shown here but shares the same trend). Further simulations confirm that additional improvements can be achieved with higher spreading factors (at the cost of a decreased data rate).

Longer Q's reduce the effective data rate, but the ability to adjust this provides flexibility. For example, more hostile channels can increase Q, effectively trading off data rate for improved robustness. We have simulated 10 transmitters operating simultaneously on a mixed LV-MV network, however, much like LoRa, many more transmitters can operate simultaneously, sharing both time and frequency resources due to the orthogonality of the chirps at various combinations of SF and bandwidth. This is an important feature of the proposed scheme given the vast and sprawling nature of MV/LV networks, and the necessity for LV feeder load data (voltage and current) from all parts of the network.

V. HARDWARE IMPLEMENTATION AND EXPERIMENTAL RESULTS

Lora-Mod-Enhanced is implemented in Field Programmable Gate Array (FPGA) hardware using the high level architecture shown in Fig. 14. The receiver is connected via UART to a Matlab App for visualisation and logging. The main features of the transmitter and receiver architectures are described next.

A. Transmitter

The FPGA based transmitter is based on a design first utilised in [16]. The baseband complex chirp (Re and Im) is stored in a pair of 32,708 point Read Only Memory (ROM) blocks. This is equivalent to an upscaling factor of 32 for a SF = 10, 1,024 point symbol. Modulation is achieved by the ROM address counter, which allows the transmitter to output phase shifted versions of the complex chirp. A Numerically Controlled Oscillator (NCO) is used to generate a carrier frequency (f_c) for quadrature mixing of the complex chirp from the baseband to the passband. A 125 MSPS Digital to Analog Converter (DAC) is used to output the passband signal and amplification is provided by the OPA564

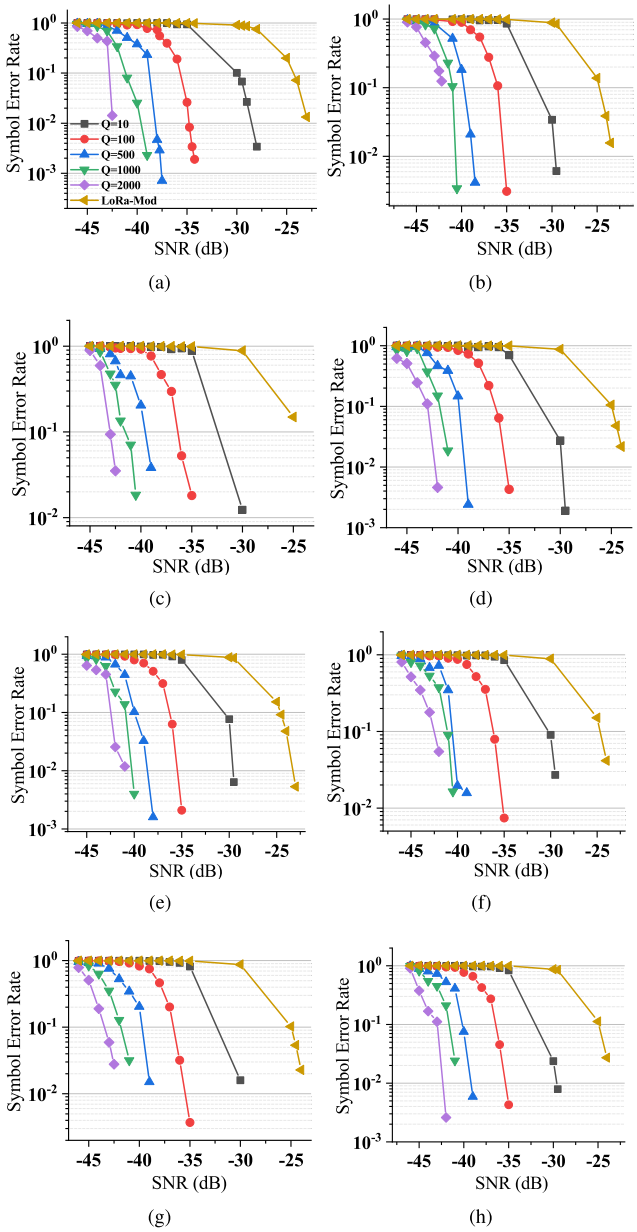

Fig. 13. SNR Versus Symbol Error Rate for SF= 13, with 7,000 runs per simulation point. Impulsive noise is added ($\alpha = 1.7$) with clipping (M = 1.3). (a) A1-O (b) A2-O (c) B1-O (d) B2-O (e) C1-O (f) D1-O (g) D2-O (h) E1-O.

Power Operational Amplifier, which is capable of driving 1.5 A at a gain-bandwidth product of 17 MHz. The LoRa bandwidth is 50 kHz.

B. Receiver

The receiver architecture shown in Fig. 14 digitises the incoming signal using a 65 MSPS, 14-bit Analog to Digital Converter (ADC), operating at a lower sampling rate of 1.6 MHz. A Gaussian Noise generator provides the option of introducing an arbitrary level of Additive White Gaussian Noise (AWGN) to the incoming signal. The core has 16-bit resolution with a random distribution of $\pm 9.1\sigma$ and a period of 2^{176}. Following downconversion and decimation by an FIR decimation filter (which downsamples the 1.6 MHz input signal by a factor of 32, down to the 50 kHz baseband), the dechirping process is carried out by a complex multiplier with a 1024-point ROM-based complex chirp.

An embedded processor is used to send the Lora-Mod output, S and the Lora-mod-enhanced output, $\mathcal{H}$ via UART (baud = 115,200 bps) to a Matlab app for visualisation and logging of the demodulated data.

To emulate a frequency selective channel, we have implemented a shift register and multiplier before the AWGN is added. This arrangements realises a simple 4-tap channel response with a separation of 4 LoRa samples between taps.

C. Experimental Results

Fig. 15 shows experimental versus simulation results obtained using the FPGA based realisation of the proposed method. Good agreement is observed for both the LoRa-Mod and LoRa-Mod-Enhanced (Q = 10, Q = 100) schemes.

Fig. 16 shows boxplots of the transmitted symbol (blue, equivalent to $\mathcal{E}$), noise symbols (red, equivalent to $\mathcal{S}$) and the averaged transmitted and noise symbols after a 10 and 100 points moving sum/average. This result was taken at SNR = -20 dB where the LoRa-Mod error rate is approximately 0.7 (large overlap between the red and blue boxes), the Q = 10 error rate is around 0.15 (small overlap) and the Q = 100 case enjoys error free communication. In this case, LoRa-Mod-Enhanced can achieve error-free communication with a time on air of $64 \cdot (2^{SF}) \cdot \left(\frac{1}{50{,}000}\right) \approx 1.3$ s per running average.

VI. Conclusion

- A new PLC modulation scheme, based on a modification of the LoRa physical layer, has been proposed. This scheme has two versions i) LoRa-Mod, which subdivides the demodulated LoRa signal into a reduced set of 'bins,' and ii) LoRa-Mod-Enhanced, which performs statistical averaging on each bin.
- The proposed scheme performs exceptionally well in the notoriously hostile LV-MV channel, coping with low SNRs, impulse noise and extreme multipath. The condition of setting the bin size to at least as great as the RMS delay spread is emphasised.
- A new simulation methodology in the ATP-EMTP was developed, allowing millions of samples and numerous transmitters to be simulated simultaneously on a mixed (LV/MV) test network. The results demonstrate robust performance in extreme multipath and SNRs as low as -40 dB, with even better performance possible at higher spreading factors and longer moving averages.
- The proposed scheme is implemented in FPGA hardware and experimental results match simulation.

Due to the nature of the proposed method, the entirety of the delayed energy resulting from the channel impulse response is contained in a single bin (in the case of LoRa-Mod-Enhanced). The data rate is deliberately slowed to ensure that a majority of the delayed energy from the multipath effect of the channel

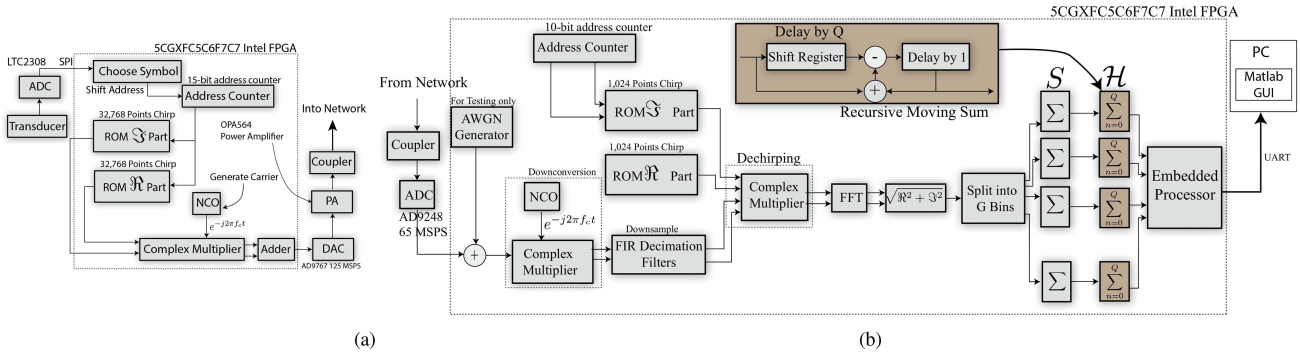

Fig. 14. FPGA based hardware architectures for the transmitter and receiver. (a) Transmitter (b) Receiver.

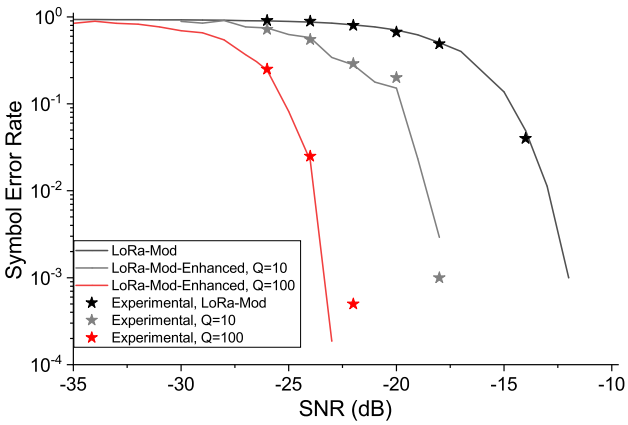

Fig. 15. Experimental versus Simulation results, where SF = 10.

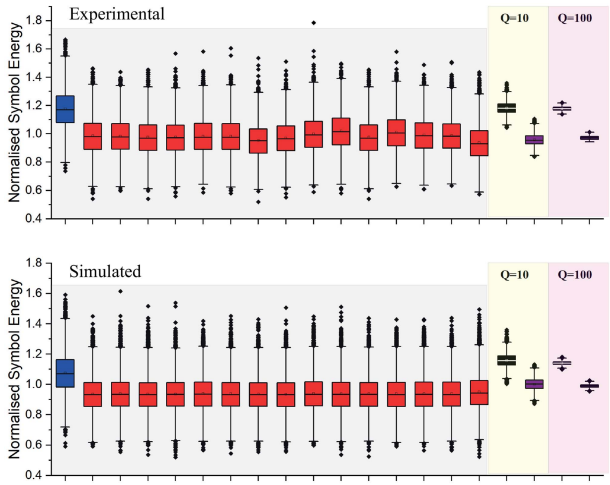

Fig. 16. Comparison of Experimental results, obtained with the FPGA prototype, and Simulation results using the same conditions. The AWGN is set to −19 dB, SF = 10.

is captured in a single symbol. Further work is required to maximise datarate for different channel conditions. Further work is also required to find the optimum threshold for clipping.

REFERENCES

[1] I. Berganza, A. Sendin, and J. Arriola, "Prime: Powerline intelligent metering evolution," in *Proc. SmartGrids Distrib.*, IET-CIRED, CIRED Seminar, 2008, pp. 1–3.

[2] K. Razazian, M. Umari, A. Kamalizad, V. Loginov, and M. Navid, "G3-PLC specification for powerline communication: Overview, system simulation and field trial results," in *Proc. IEEE Int. Symp. Power Line Commun. Appl.*, 2010, pp. 313–318.

[3] S. Robson, M. Haddad, and H. Griffiths, "A new methodology for the simulation of emerging power line communication standards," *IEEE Trans. Power Del.*, vol. 33, no. 3, pp. 1025–1034, Jun. 2018.

[4] J. Meng and A. E. Marble, "Effective communication strategies for noise-limited power-line channels," *IEEE Trans. Power Del.*, vol. 22, no. 2, pp. 887–892, Apr. 2007.

[5] D. Radford, "Spread spectrum data leap through ac power wiring," *IEEE Spectr.*, vol. 33, no. 11, pp. 48–53, Nov. 1996.

[6] Semtech, *LoRa Modulation Basics: Application Note*, Semtech, May 2015.

[7] Y. Xiaoxian, Z. Tao, Z. Baohui, N. H. Xu, W. Guojun, and D. Jiandong, "Investigation of transmission properties on 10-KV medium voltage power lines–part I: General properties," *IEEE Trans. Power Del.*, vol. 22, no. 3, pp. 1446–1454, Jul. 2007.

[8] H. Gassara, F. Rouissi, and A. Ghazel, "Statistical characterization of the indoor low-voltage narrowband power line communication channel," *IEEE Trans. Electromagn. Compat.*, vol. 56, no. 1, pp. 123–131, Feb. 2014.

[9] R. Lefort, R. Vauzelle, V. Courtecuisse, N. Idir, and A.-M. Poussard, "Influence of the MV/LV transformer impedance on the propagation of the PLC signal in the power grid," *IEEE Trans. Power Del.*, vol. 32, no. 3, pp. 1339–1349, Jun. 2017.

[10] T. Bai *et al.*, "Fifty years of noise modeling and mitigation in power-line communications," *IEEE Commun. Surv. Tut.*, vol. 23, no. 1, pp. 41–69, Jan.-Mar. 2021.

[11] B. Adebisi, K. Anoh, K. M. Rabie, A. Ikpehai, M. Fernando, and A. Wells, "A new approach to peak threshold estimation for impulsive noise reduction over power line fading channels," *IEEE Syst. J.*, vol. 13, no. 2, pp. 1682–1693, Jun. 2019.

[12] S. V. Zhidkov, "Analysis and comparison of several simple impulsive noise mitigation schemes for OFDM receivers," *IEEE Trans. Commun.*, vol. 56, no. 1, pp. 5–9, Jan. 2008.

[13] Y.-R. Chien, "Iterative channel estimation and impulsive noise mitigation algorithm for OFDM-based receivers with application to power-line communications," *IEEE Trans. Power Del.*, vol. 30, no. 6, pp. 2435–2442, Dec. 2015.

[14] S. Robson and A. M. Haddad, "On the use of LoRa for power line communication," in *Proc. 54th Int. Universities Power Eng. Conf.*, 2019, pp. 1–6.

[15] S. Rinaldi *et al.*, "Design of a time dissemination system using chirp modulation for medium voltage smart grid applications," *IEEE Trans. Instrum. Meas.*, vol. 69, no. 9, pp. 6686–6695, Sep. 2020.

[16] S. Robson and A. M. Haddad, "Development of an fpga based time of arrival estimator for plc applications," in *Proc. 55th Int. Universities Power Eng. Conf.*, 2020, pp. 1–6.

[17] L. Vangelista, "Frequency shift chirp modulation: The LoRa modulation," *IEEE Signal Process. Lett.*, vol. 24, no. 12, pp. 1818–1821, Dec. 2017.

[18] U. Raza, P. Kulkarni, and M. Sooriyabandara, "Low power wide area networks: An overview," *IEEE Commun. Surv. Tut.*, vol. 19, no. 2, pp. 855–873, Apr.-Jun. 2017.

[19] T. Elshabrawy and J. Robert, "Closed-form approximation of lora modulation ber performance," *IEEE Commun. Lett.*, vol. 22, no. 9, pp. 1778–1781, Sep. 2018.

[20] Y. Guo and Z. Liu, "Time-delay-estimation-liked detection algorithm for lora signals over multipath channels," *IEEE Wireless Commun. Lett.*, vol. 9, no. 7, pp. 1093–1096, Jul. 2020.

[21] M. Tlich, A. Zeddam, F. Moulin, and F. Gauthier, "Indoor power-line communications channel characterization up to 100 MHz–part I: One-parameter deterministic model," *IEEE Trans. Power Del.*, vol. 23, no. 3, pp. 1392–1401, Jul. 2008.
[22] A. Mathur, M. R. Bhatnagar, and B. K. Panigrahi, "Plc performance analysis over rayleigh fading channel under nakagami-m additive noise," *IEEE Commun. Lett.*, vol. 18, no. 12, pp. 2101–2104, Dec. 2014.
[23] G. Laguna-Sanchez and M. Lopez-Guerrero, "On the use of alpha-stable distributions in noise modeling for PLC," *IEEE Trans. Power Del.*, vol. 30, no. 4, pp. 1863–1870, Aug. 2015.
[24] L. Bai, M. Tucci, S. Barmada, M. Raugi, and T. Zheng, "Impulsive noise characterization in narrowband power line communication," *Energies*, vol. 11, no. 4, 2018, Art. no. 863. [Online]. Available: https://www.mdpi.com/1996-1073/11/4/863
[25] T. H. Tran, D. D. Do, and T. H. Huynh, "PLC impulsive noise in industrial zone: Measurement and characterization," *Int. J. Comput. Elect. Eng.*, vol. 5, no. 1, pp. 48–51, 2013.
[26] J. Wang, E. E. Kuruoglu, and T. Zhou, "Alpha-stable channel capacity," *IEEE Commun. Lett.*, vol. 15, no. 10, pp. 1107–1109, Oct. 2011.
[27] A. Cataliotti, V. Cosentino, D. Di Cara, and G. Tine, "Oil-filled MV/LV power-transformer behavior in narrow-band power-line communication systems," *IEEE Trans. Instrum. Meas.*, vol. 61, no. 10, pp. 2642–2652, Oct. 2012.

Stephen Robson (Member, IEEE) received the M.Eng. and Ph.D. degrees in 2007 and 2012, respectively. Between 2007 and 2008, he was a Graduate Engineer with National Grid U.K. In 2013, he was appointed as a Lecturer, and since 2020, he has been a Senior Lecturer of electrical engineering with Cardiff University, Cardiff, U.K. His main research interests include power line communication, fault location, earthing systems, condition monitoring, and simulation of transients on electrical networks. He is a member of BSI GEL/81 standards committee (Protection against Lightning).

Manu Haddad (Member, IEEE) received the Ingénieur d'État degree in electrical engineering and the Ph.D. degree in high-voltage engineering in 1985 and 1990, respectively. He is currently a Professor of electrical engineering with Cardiff University, Cardiff, U.K., responsible for research in high-voltage engineering. He has authored an IET- Power Series Book entitled *Advances in High-Voltage Engineering*. His research interests include overvoltage protection, insulation systems, insulation coordination, and earthing of electrical energy systems. He is a member of several CIGRE Working Groups and a member of the BSI PEL1/2, IEC TC37, and IEC ACTAD committees MT4 and MT10. He is on the scientific committees of several international conferences. He is a Fellow of the IET and the Learned Society of Wales.